

## Material properties

# Improved thermo-oxidative stability of three-dimensional and four-directional braided carbon fiber/epoxy hierarchical composites using graphene-reinforced gradient interface layer



Wei Fan, Jia-lu Li\*, Yuan-yuan Zheng

Composite Research Institute of Tianjin Polytechnic University, Tianjin and Education Ministry Key Laboratory of Advanced Textile Composite Materials, Tianjin 300387, China

## ARTICLE INFO

## Article history:

Received 7 March 2015

Accepted 12 April 2015

Available online 29 April 2015

## Keywords:

Polymer-matrix composite (PMC)

Interface/interphase

Thermo-oxidative aging

Mechanical testing

Graphene

Atomic force microscopy (AFM)

## ABSTRACT

In order to improve the thermo-oxidative stability of three-dimensional and four-directional braided carbon fiber/epoxy composites, we introduced a gradient interphase reinforced by graphene nanoplatelets (GN) between the carbon fiber and the matrix, with a liquid phase deposition strategy. Both the interlaminar shear strength and the flexural strength of the composites were improved after thermo-oxidative aging at 140 °C for various durations (up to 1200 h). The interfacial reinforcing mechanisms are explored by analyzing the structure of the interfacial phase, thermal conductivity, weight loss, surface topography, fiber/matrix interfacial morphology and thermomechanical properties of the composites. Results indicate that the GN-reinforced gradient interphase provides an effective shield against interface oxidation, assists in thermal stress transfer, and restricts the movement of the different phases of materials at the composite interface.

© 2015 Elsevier Ltd. All rights reserved.

## 1. Introduction

Carbon fiber (CF) polymer matrix composites (PMCs) are extensively employed in the aerospace industry owing to their high specific mechanical properties [1]. However, degradation of the properties of the constituents, i.e., fiber, matrix and fiber/matrix interphase, occurs when the CFPMCs are exposed to oxidative environments at high temperatures. In particular, fiber/matrix interface oxidation governs the oxidation rate of the CFPMCs [2,3]. For traditional laminated composites, the occurrence and development of microscopic damage (fiber/matrix debonding or micro-cracks) promote delamination [4], which degrades the structural properties and reduces service life of

CFPMCs. However, the emergence of new advanced aerospace applications (“hot” structures) has given a new impetus to the development of CFPMCs with higher thermo-oxidative stability (TOS).

Compared to conventional laminated composites, the integrated structure of three-dimensional (3D) and four-directional (4Dir) braided composites can improve the TOS of the CFPMCs by enhancing the ability of the fibers to bear the external load and resist delamination, despite the deterioration in the matrix resin and interface properties after thermo-oxidative aging (TOA) for long periods of time [5]. Unfortunately, however, the flexural strength (FS) of the 3D-4Dir braided composite decreases significantly when the fiber/matrix interface performance declines extensively after TOA [6].

Although substantial research has been conducted on improving the interface performance of CFPMCs, only a small portion has focused on the effect of interface

\* Corresponding author. Tel.: +86 022 24528052; fax: +86 022 24528448(4).

E-mail address: [lijialu@tjpu.edu.cn](mailto:lijialu@tjpu.edu.cn) (J.-l. Li).

performance on the TOS of CFPMCs [3,7]. Bowles [7] studied the effects of fiber surface modification on the TOS of Graphite/PMR-15 composites and noted that the AS-4G composites exhibited a higher interlaminar shear strength (ILSS) compared to AS-4 composites at room temperature. However, after TOA, the ILSS of the AS-4G composites (in the above study) was somewhat worse than that of the AS-4 composites. This was attributed to the 1.5 % low temperature epoxy sizing at the fiber/matrix interface of the AS-4G composites. The low temperature epoxy sizing on the fiber surfaces degraded rapidly, resulting in diffusion of air along the fiber/matrix interfaces, accelerating the interface oxidation. This example illustrates that the CFPMCs with higher bonding strengths at room temperature do not necessarily have higher TOS after TOA. Furthermore, it demonstrates that the TOS of the reinforced material itself has a great influence on the TOS of CFPMCs. The introduction of GN into conventional continuous fiber reinforced PMCs to create hierarchical reinforcement structures is currently of significant interest owing to the GN's unique structure, outstanding strength and modulus, and excellent electrical and thermal properties [8,9]. Recent research demonstrates that, by incorporating GN, significant improvements are achieved in CFPMCs, especially for the fiber/matrix interphase and the matrix-dominated out-of-plane performance, such as interfacial shear strength [8,10], impact strength [8] and fatigue resistance [9]. However, there are few studies on the properties of GN-reinforced CFPMCs after TOA.

Therefore, the purpose of the current investigation was to determine the role of a GN-reinforced hierarchical interface on the TOS of a 3D-4Dir braided/epoxy composite. The specimens were thermally oxidized at 140 °C for various durations. After exposure to the high temperature, composites were characterized to: (1) determine the weight loss and reduction in FS and ILSS at different exposure times, (2) observe the corresponding microcracks and surface damage, and (3) understand the reinforcement mechanism of the GN-reinforced hierarchical interface.

## 2. Experimental details

### 2.1. Materials

T700-12K CF (Toray) was used for this study. An epoxy resin JC-02A based on diglycidyl ether of bisphenol A (Changshu Jaffa Chemical Co., Ltd.) with hardener JC-02B (improved methyl tetrahydrophthalic anhydride) and accelerant JC-02C (tertiary amine) was used for the matrix. Graphite powder with an average diameter of 10  $\mu\text{m}$  was purchased from Qingdao AoKe ShiMo Co. Ltd., China. Concentrated  $\text{H}_2\text{SO}_4$  (98%), concentrated  $\text{H}_3\text{PO}_4$  (85%),  $\text{KMnO}_4$ , acetone and 30%  $\text{H}_2\text{O}_2$  (Tianjin Fengchuan Co., Ltd.) were used to make the GN.

### 2.2. Preparation of GN-coated CFs

The processes for making graphite oxide (GO), GN, and GN-coated CFs are detailed in reference [11]. The difference between the GN-coated CFs used in our study and those in reference [11] is that the former were made with commercial CFs without any treatment. The CFs absorbed 1 wt.% GN, relative to the composites. A GN concentration of 1 wt.% was chosen because previous researchers [11] have shown that this proportion is the best choice to improve the FS and ILSS of CF/epoxy composites at room temperature.

### 2.3. Preparation of 3D-4Dir braided CF/epoxy composites (BCs), 3D-4Dir braided GN-coated CF/epoxy composites (BGCs), and neat resin (NR)

Both the 3D-4Dir braided commercial CF preforms and 3D-4Dir braided GN-coated CF preforms were manufactured by the intertwining or orthogonal interlacing of four sets of yarns-braiders to form a 3D sheet fabric [12]. The 3D-4Dir braided architecture is illustrated in Fig. 1(c). It is characterized by almost all the braider yarns being offset at different angles between the in-plane and through-thickness directions, which can be seen clearly from the

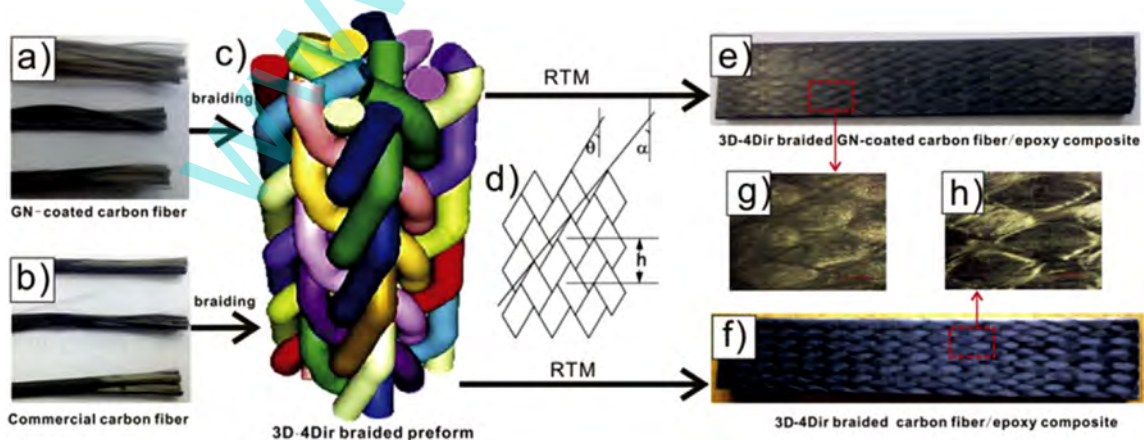


**Fig. 1.** Graphene nanoplatelet(GN)-coated carbon fibers(CFs) (a), commercial CFs (b), three-dimensional(3D) and four-directional(4Dir) braided architecture (c), an idealized model of the 3D-4Dir braided preform surface (d), a flexural specimen of 3D-4Dir braided GN-coated CF/epoxy composites (BGCs) (e) and 3D-4Dir braided CF/epoxy composites (BCs) (f), zoom on the surface of BGCs (g) and BCs (h).

tracer yarn (colored yarns). An idealized model of the braid preform surface is shown in Fig. 1(d), where  $h$  is the braiding pitch length,  $\theta$  is the surface braiding angle and  $\alpha$  is the braiding angle. The average braiding angle,  $\alpha$ , of the 3D-4Dir braided preforms in this study was  $22.3^\circ$ . The production process for the BGCs was the same as that for the BCs, the only difference being that the fibers used for the BCs were commercial CFs (Fig. 1(b)), whereas those used for the BGCs were the GN-coated CFs (Fig. 1(a)). The production processes for the composites and the neat resin are covered elsewhere [6]. The final specimens of the BGCs and BCs are illustrated in Fig. 1(e) and (f), respectively. The average fiber volume fraction in the BGCs and BCs was approximately 55%.

#### 2.4. Accelerated aging experiments

In order to evaluate the TOS of the composites, an accelerated TOA procedure was adopted according to ISO 2578-1998. Specimens were isothermally aged at  $140^\circ\text{C}$  for 168, 360, 720, and 1200 h. After heating for a given aging time, the specimens were removed and cooled in a desiccator to avoid moisture absorption. The specimens were stored at  $25 \pm 3^\circ\text{C}$  for at least 24 h prior to testing.

#### 2.5. Tests

The surface topography of CFs and the cross-sections of the composite specimens were examined using a Hitachi S-4800 field emission scanning electron microscope (FE-SEM). Atomic force microscopy (AFM) of the composites was performed using a CSPM 5500 scanning probe microscope. After flexural testing, the fracture surface morphology of the composites was examined in a VHX-1000 3D microscopy system. A JEOL TM-100 SEM was employed to observe the fiber/matrix interfacial morphology of the composites.

Thermal conductivity of the composites was measured with a TC 3010 apparatus (Xi'an Xiotech Electronic Technology Co. Ltd., China), in accordance with ISO 22007-2-2008. Thermal conductivity tests were conducted at  $25^\circ\text{C}$ , on specimens with dimensions of  $40\text{ mm} \times 30\text{ mm} \times 4\text{ mm}$ .

An electronic balance with 0.1 mg accuracy was used for recording the weight loss of the composites. The testing method is detailed elsewhere [13].

Dynamic mechanical analysis (DMA) was conducted on the specimens to investigate the  $T_g$ , according to ISO 6721-11-2012, using three-point bending. The tests were performed in the scanning temperature mode, in the range from  $40$  to  $185^\circ\text{C}$ , at a heating rate of  $5^\circ\text{C}/\text{min}$ , and with an oscillating frequency of 1.0 Hz. Three specimens, rectangular in shape with a nominal size of  $60\text{ mm} \times 10\text{ mm} \times 2\text{ mm}$ , were analyzed for each level of thermal treatment.

The flexural specimens (80 mm length, 15 mm width and 4 mm thickness) were first used for the weight loss test. The flexural tests were conducted in accordance with ISO 14125-1998 using a three-point loading method. The ILSS of specimens (20 mm length, 10 mm width, and 2 mm thickness) was determined by a three-point short beam shear test, in accordance with ISO 14130-1997. The mechanical tests were conducted at  $23^\circ\text{C}$  and 50% relative

humidity, and each data point indicated in the results is an average of three separate measurements.

### 3. Results and discussions

#### 3.1. Surface topography and stiffness distribution of the hierarchical interphase

To verify the introduction of hierarchical layers, the interfacial phase structures of the pristine and the multi-scale composites with 1 wt.% GN were examined in detail. The surface morphologies of CF, before and after depositing GN, as observed by FE-SEM, are shown in Figs. 2(a) and 3(a), respectively. It is seen that the commercial T700 CF had a smooth surface. After absorption, most of the GNs were attached to the fiber surface (Fig. 3(a)), revealing the formation of a new hierarchical structure [14]. Figs. 2(b) and 3(b) are schematic representations of the unit cell that constitutes the 2-phase (CF/epoxy) composite (BC) and the 3-phase (CF/GN/epoxy) hierarchical composite (BGC), respectively. Linear scans were conducted in FE-SEM to evaluate the distribution of elements in the interface region, and the results are shown in Figs. 2 and 3. As illustrated in Fig. 2(d), a sudden drop in elemental carbon concentration can be observed going from the CF to the epoxy. However, this drop became much slower after the addition of GN (Fig. 3(d)), which demonstrates the formation of a nano-composite interface layer reinforced by GN in the CF/epoxy interfacial phase. In addition, elemental carbon concentration dwindled steadily from the CFs to the epoxy, indicating a gradient distribution of GN in the BGC and supporting the construction of gradient interface layers. The thickness of these layers was  $\sim 0.98\ \mu\text{m}$  (Fig. 3(d)).

For further investigation of the interfacial phase structures of composites, the force modulation mode of AFM was adopted to study the stiffness of various phases of composites. This further allowed a qualitative probe of the local modulus of the specimen surface, using an oscillating cantilever tip that indented the specimen surface. The corresponding cantilever amplitude changes under scanning in accordance with the local modulus of the specimen. Since compliant areas undergo larger indentation than stiffer areas of the specimen, different responses to the cantilever from areas with different modulus can be observed [15,16]. However, because only two external channels were available, only the amplitude of the electrical AC current signal and the amplitude of the mechanical AC signal could be recorded [16]. Therefore, the relative stiffness value was indirectly indicated by the voltage generated from the cantilever deflection. Figs. 2(e) and 3(e) show the relative stiffness images of cross-sectional areas in the BC and BGC, respectively. The relative stiffness image of the CF was brighter than that of the surrounding epoxy, implying that the stiffness of the CF was higher than that of the epoxy. Furthermore, the relative stiffness image displayed a clear distinction between the CF and the surrounding epoxy (Fig. 2(e)). After incorporation of GNs, the boundary between the CF and the epoxy became more blurred (Fig. 3(e)). Figs. 2(f) and 3(f) represent the corresponding relative stiffness distribution curves of the cross-sectional areas in Figs. 2(e) and 3(e), respectively. There was

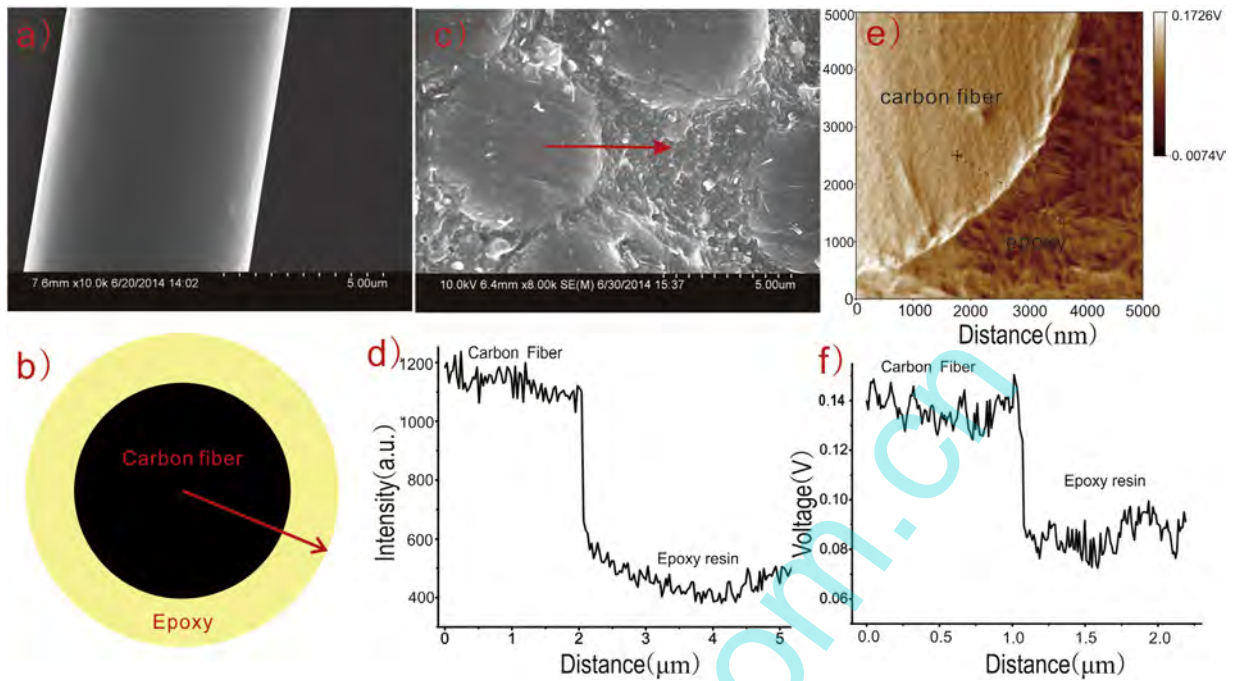


**Fig. 2.** (a) The surface morphologies of the raw CF, (b) schematic representations of the unit cell that constitutes the 2-phase (CF/epoxy) composite (BC), (c) FE-SEM image of cross-sectional areas in the BC, (d) elemental carbon concentration varying from the CF to the epoxy along the direction of arrow in (c), (e) the relative stiffness image of cross-sectional areas in the BC, (f) the relative stiffness distribution curve of the cross-sectional area in the BC corresponding to (e).

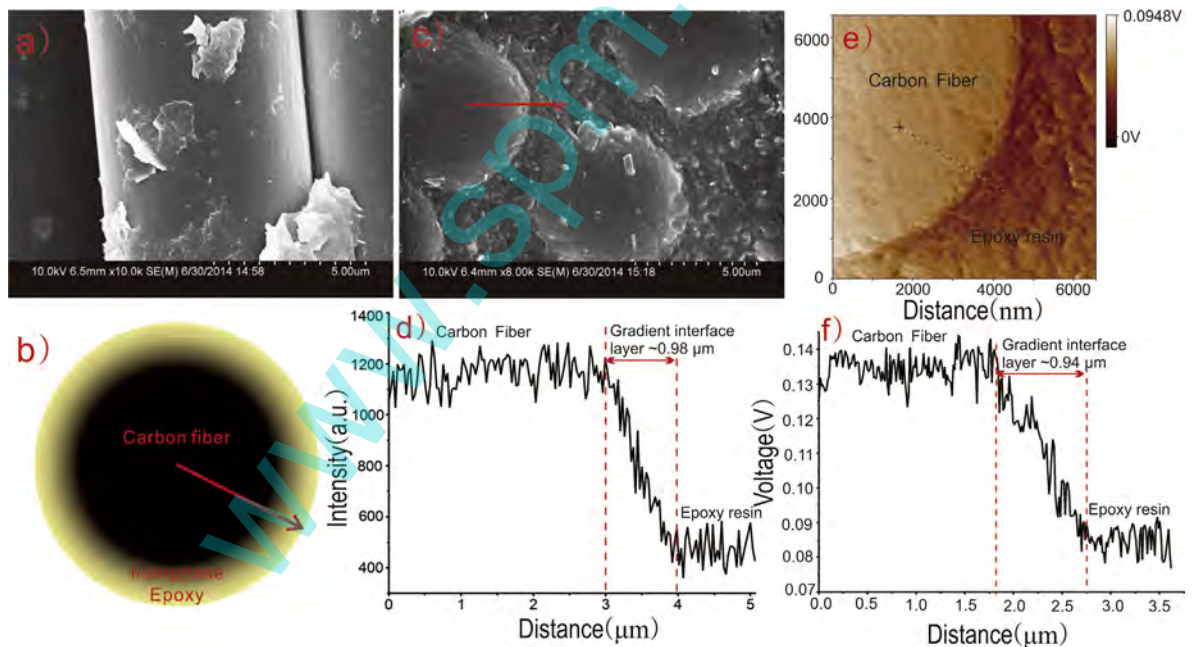


**Fig. 3.** (a) The surface morphologies of the GN-coated CF, (b) schematic representations of the unit cell that constitutes the 3-phase (CF/GN/epoxy) hierarchical composite (BGC), (c) FE-SEM image of cross-sectional areas in the BGC, (d) elemental carbon concentration varying from the CF to the epoxy along the direction of arrow in (c), (e) the relative stiffness image of cross-sectional areas in the BGC, (f) the relative stiffness distribution curve of the cross-sectional area in the BGC corresponding to (e).

a sharp drop in stiffness from CF to epoxy for the BC (Fig. 2(f)). Again, this drop became more gradual after adding GN, which implied the introduction of a gradient interface layer in good agreement with the linear FE-SEM

results. The interphase thickness value was  $\sim 0.94 \mu\text{m}$  (Fig. 3(f)), which is a little smaller than that in Fig. 3(d), most probably due to specimen disparity and experimental errors.

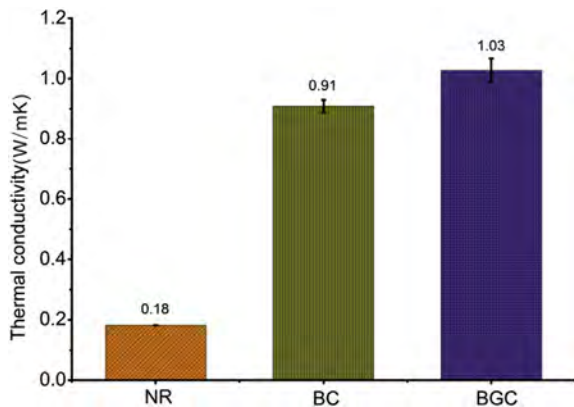


Fig. 4. Thermal conductivity of neat resin (NR), 3D-4Dir braided CF/epoxy composite (BC), and 3D-4Dir braided GN-coated CF/epoxy composite (BGC).

### 3.2. Thermal conductivity analysis

Fig. 4 shows that the thermal conductivity of the NR, BC, and BGC was 0.18, 0.91, and 1.03 W/mK, respectively. In this study, the thermal conductivity of the BC and BGC was measured along the width of the specimens (i.e., transverse thermal conductivity of the composites). Compared to the BC, the thermal conductivity of the BGC was 13% higher owing to the addition of GNs (1 wt.%) with a high thermal conductivity (5000 W/mK) [17].

### 3.3. Weight loss analysis

Since the oxidation process is sensitive to the surface area of the different test specimens [18], the TOA data are presented in terms of weight loss per unit surface area of the specimens as a function of aging time (see Fig. 5). Note that, for both types of composites, the weight loss increased with aging time. However, the overall weight loss as well as the rate of weight loss was higher in the BCs than in the BGCs. Two reasons may account for this phenomenon. Firstly, the

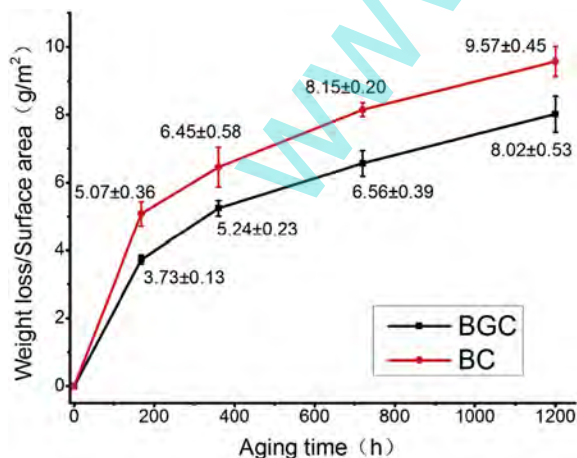
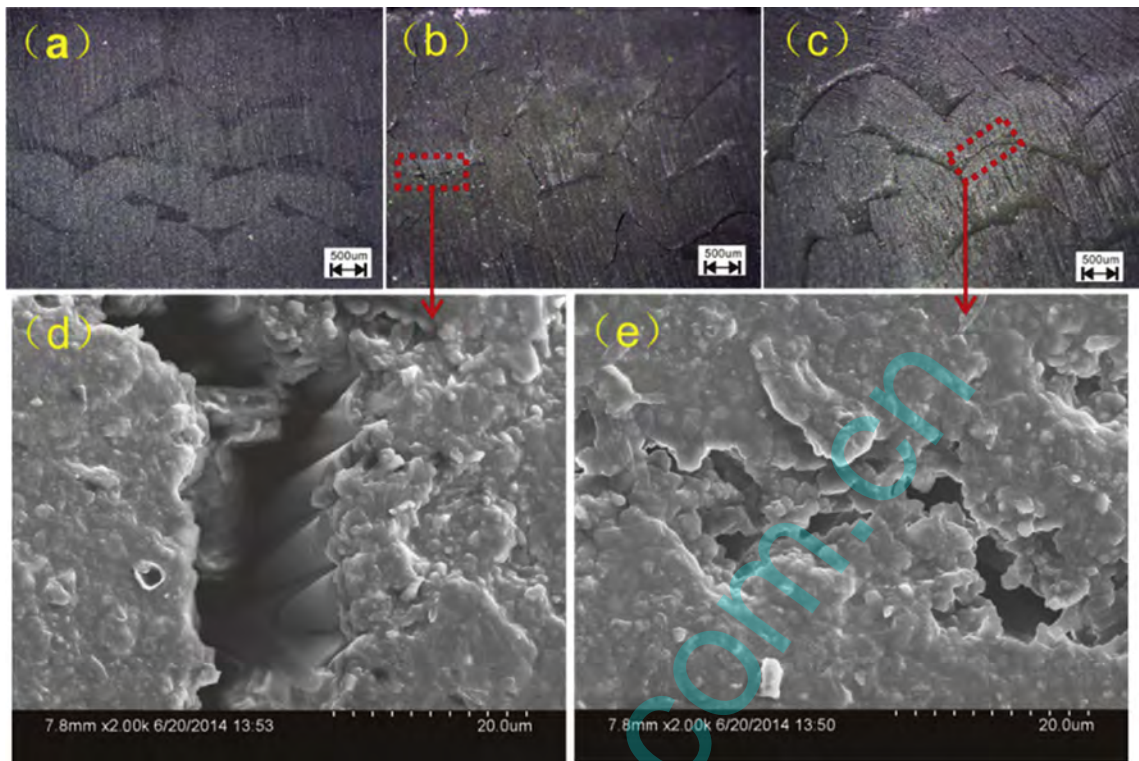


Fig. 5. Weight loss per unit surface area of the BC and BGC specimens vs. aging time at 140 °C.

GN produced by the thermal reduction of GO [19] could have residual hydroxyl and epoxide functional groups, which could interact covalently with the epoxy chains, thereby furthering interfacial adhesion. A strong interface can hinder the diffusion of oxygen into the composites, reducing the oxidation weight loss of the interface [3]. Secondly, the axial (100 W/mK) and radial thermal conductivity (11 W/mK) of the T700 CF [20] were 555 and 61 times as high, respectively, as the value for the NR (0.18 W/mK). Mismatches in the thermal conductivity between the CF and the matrix give rise to localized thermal stresses at the fiber–matrix interface, which makes it prone to micro-cracks. After adding GN at the fiber–matrix interface in CF/epoxy composites, the thermal conductivity of the BGC was improved by 13% compared to that of the BC. The elemental carbon content dwindled steadily from the CF to the epoxy (Fig. 3(d)), indirectly indicating that the thermal conductivity of the GN-reinforced gradient interphase layer was lower than that of the CF and higher than that of the matrix. Such a gradient conductive layer could transfer the interfacial thermal stress, mitigating the interfacial damage. The cross-sectional photomicrographs and SEM pictures of the fracture surfaces of the un-aged and aged specimens, in Figs. 6 and 7, may be good evidence for the two explanations above about the potentiation of GNs. No damage is observed on the un-aged specimen surface (Fig. 6(a)), but many micro-cracks appear on the end cross-section of the aged specimen (Fig. 6(b)). The micro-cracks are also noted on the end cross-section of the BGC (Fig. 6(c)). However, in comparison to the BC, the extent of micro-cracks is much less in the BGC specimens. By comparing Fig. 6(d) and (e), it can be seen that micro-cracks in BCs are more open than in BGCs, and the fiber–matrix debonding onset (Fig. 6(d)) is observed clearly. Fig. 7 shows the typical SEM pictures of the fracture surfaces of un-aged and aged BC (left) and BGC (right). On the fracture surfaces of both un-aged specimens (Fig. 7(a) and (f)), the fibers are covered with the matrix, indicating good adhesion between fiber and matrix. However, the adhesion between fiber and matrix on the fracture surface of BGCs seems to be better than that in BCs, which indicates that GN can promote interfacial adhesion. In aged BC specimens, the cracks propagated almost entirely along the fiber/matrix interface after aging for 168 h (Fig. 7(b)). After aging for 360 h, the amount of resin attached to the fibers decreased, and grooves were formed due to fiber pull out (Fig. 7(c)). With further increase in aging time, fibers were loose, and the fiber surfaces were completely devoid of matrix material (Fig. 7(d) and (e)). Significant interfacial failure was also noted in the fracture surfaces of composites with GN-coated fibers. However, in comparison to the BC specimens, the extent of the interfacial failure was much less in the BGC specimens. The fibers on the fracture surfaces of the BGC specimens were still held together by the matrix resin after aging for 720 h (Fig. 7(i)). Furthermore, although the fibers had pulled loose after aging for 1200 h (Fig. 7(j)), matrix resins were still present, filling the space between the fibers. The photomicrographs and SEM analyses reveal that the GN-reinforced gradient interphase layer in BGCs not only promotes interfacial adhesion, but also facilitates the transfer of interfacial thermal stress, mitigating interface damage.



**Fig. 6.** The cross-sectional photomicrographs of the un-aged (a) and aged BC (b) and BGC (c). (d) Zoom on thermo-oxidation induced micro-cracks corresponding to (b), and (e) Zoom on thermo-oxidation induced micro-cracks corresponding to (c).

#### 3.4. Thermomechanical property analysis

Polymer materials undergo a maximum change in the mobility of polymer chains at a temperature corresponding to the peak maximum of loss modulus, defined as  $T_g$  [21]. The values for  $T_g$  were extracted from the DMA traces (see Fig. 8). The  $T_g$  for the un-aged BGC (146.5 °C) was about 5 °C higher than that of the BC (141.9 °C). There are two possible reasons for this observation. One is that the interface bonding performance of BGCs is better than that of BCs, and a strong interface can restrict the movement of different phases of the materials at the interfaces. The other is the rough and wrinkled surface topology of GN-modified CF (Fig. 3(a)), which facilitates mechanical interlocking, thereby increasing the interfacial friction and restricting the movement of the different phases of the materials at the interfaces [15]. Additionally, the  $T_g$  for all the BCs and BGCs decreased with longer aging times owing to the scission degradation of the matrix resin [22]. However, the degree of drop in  $T_g$  for the BC was higher than that for the BGC. For example, after aging for 1200 h at 140 °C, the  $T_g$  for the BC decreased by 7.3 °C, which was greater than the decrease for the BGC (4.5 °C). This is because the GN enhanced gradient interface layer effectively alleviates the interface oxidation in BGCs.

#### 3.5. Mechanical properties analysis

The thermo-oxidative degradation of CFPMCs is mainly controlled by the matrix and fiber/matrix oxidation

[4,23–25], and the FS and ILSS of CFPMCs are very sensitive to the matrix strength and the interfacial bonding between the fiber and matrix [26,27]; hence, FS and ILSS were chosen as positive indicators of thermo-oxidative degradation.

The ILSS and FS values for the two un-aged composites are shown in Fig. 9(a) and (b), respectively. With the small addition of GN (1 wt.%), the ILSS increased from 59.86 MPa in the BC to 70.79 MPa in the BGC (Fig. 9(a)), an 18% increase. Similarly, the FS increased from 724.01 MPa in the BC to 832.57 MPa in the BGC (Fig. 9(b)), a 15% increase. The probable rationale for the interfacial reinforcement by GNs is summarized as follows: (1) the stiffness of the gradient interphase is lower than that of the CF and higher than that of the epoxy. The gradient in stiffness results in the gradient interphase acting as a stress transfer medium, transferring the load from the epoxy to the CFs more uniformly, (2) the rough and wrinkled surface topology of the GN-modified CF enables it to mechanically interlock, increasing the interfacial friction and restricting the movement of the different phases of materials at the composite interfaces, and (3) GN produced by the thermal reduction of GO [19] might have residual hydroxyl and epoxide functional groups which could interact covalently with the epoxy chains, thereby further promoting interfacial adhesion. The good interfacial bonding can probably prevent oxygen penetration deep into the composite along the fiber/matrix interface during the TOA process, reducing oxidation of the interface.

In order to compare the TOS of the two composites, the normalized method was used to analyze the ILSS and FS

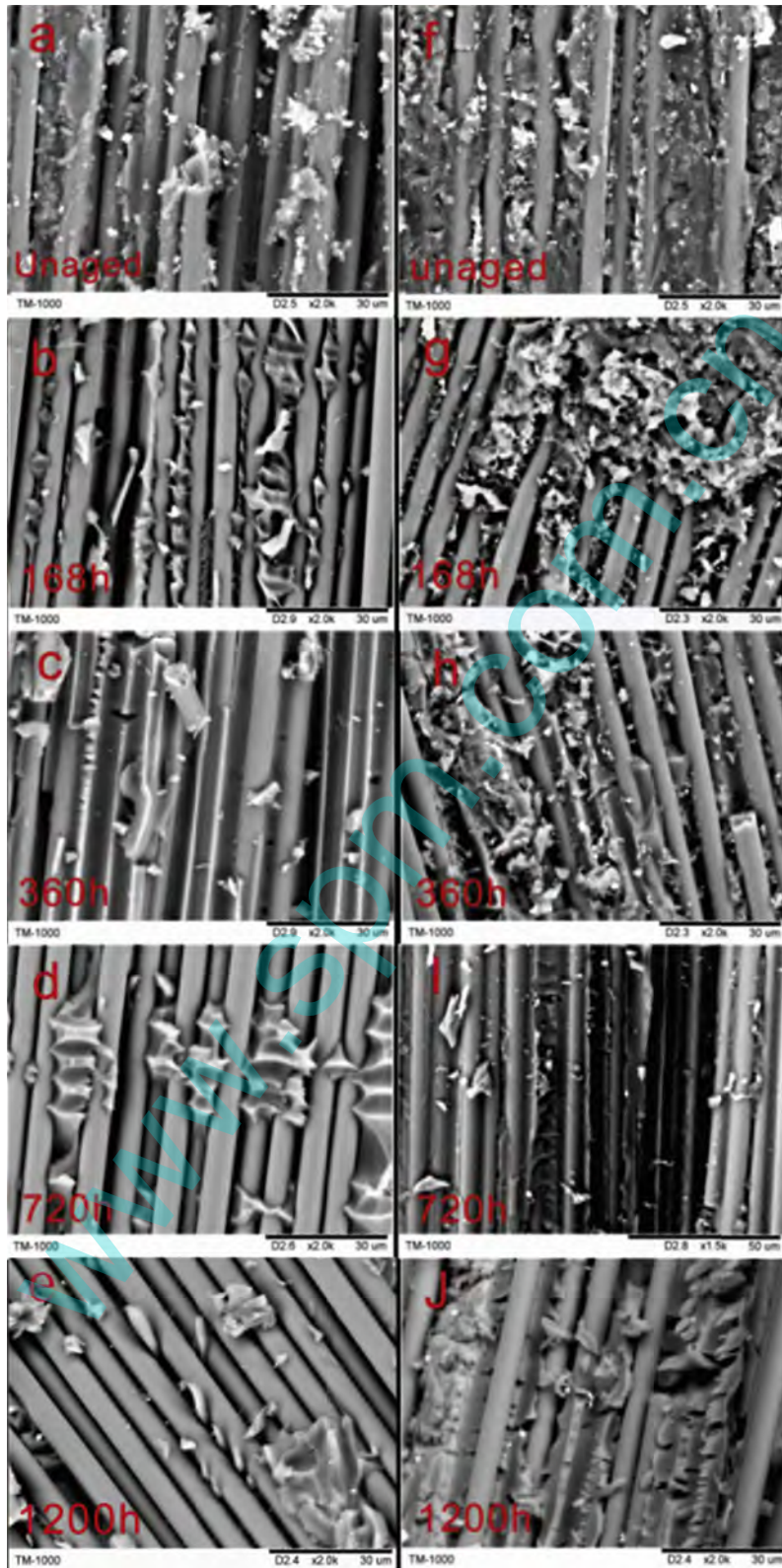


Fig. 7. SEM pictures of the fracture surfaces of the unaged and aged (1200 h at 140 °C) BC (left) and BGC (right).

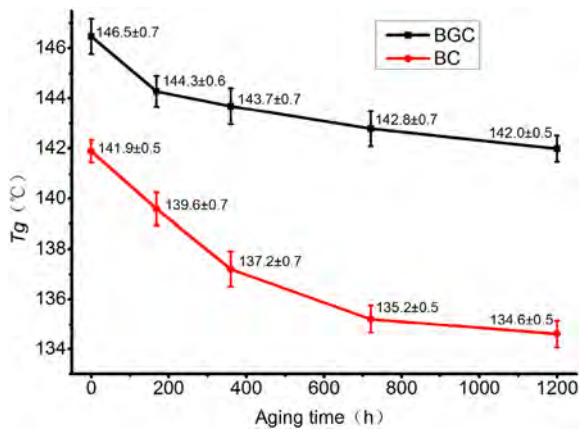


Fig. 8. The  $T_g$  for BC and BGC vs. aging time at 140 °C.

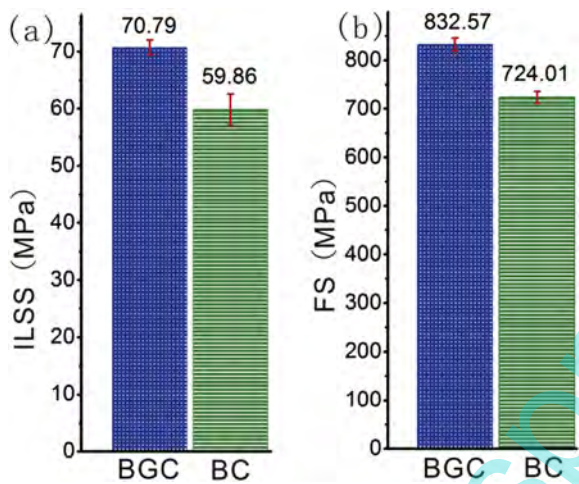


Fig. 9. Interlaminar shear strength (ILSS) (a) and flexural strength (FS) (b) of the unaged BGC and BC.

data. Fig. 10(a) and 10(b) show the normalized ILSS and FS of the two composites, respectively. In both the BC and the BGC, a decrease in FS and ILSS was observed with increasing aging time, which can be attributed to the

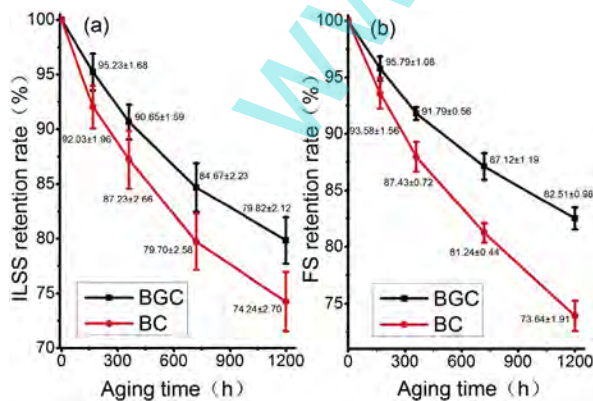


Fig. 10. ILSS (a) and FS (b) retention rate of BC and BGC vs. aging time at 140 °C.

progressive deterioration of the matrix and fiber/matrix interface caused by the TOA in the form of weight loss, micro-cracks and fiber/matrix debonding. However, under the same aging conditions, the ILSS and FS retention rates for the BGC were higher than those for the BC. For example, after aging for 1200 h, the ILSS retention rate for the BGC (80%) was 6% higher than that for the BC (74%). Similarly, the FS retention rate for the BGC (83%) was 9% higher than that for the BC (74%). This is due to the reinforcing effect of the GN, which is probably due to the reasons specified previously.

#### 4. Conclusions

This study investigates the effect of a graphene nanoplatelet (GN)-reinforced gradient interface on the thermo-oxidative stability (TOS) of three-dimensional (3D) and four-directional (4Dir) braided carbon fiber/epoxy composites before and after thermo-oxidative aging (TOA). Before TOA, the interlaminar shear strength (ILSS) and flexural strength (FS) of the 3D-4Dir braided GN-coated carbon fiber/epoxy composites (BGCs) increased by 18% and 15%, respectively, compared to the values for the 3D-4Dir braided CF/epoxy composites (BCs). This increase relates to the fact that the GN-reinforced gradient interphase may promote stress transfer from the epoxy to the carbon fibers more uniformly, restrict the movement of different phases of the materials at the interface, and promote interfacial adhesion. After exposure to 140 °C, the ILSS and FS of the two composites decreased with increase in aging time due to the deterioration of the matrix and fiber–matrix interface, in the form of weight loss, micro-cracks and fiber/matrix debonding. However, under the same aging conditions, the FS and ILSS of the BGCs were higher than those of the BCs. For example, after aging for 1200 h, the ILSS and FS retention rates for the BGC were 6% and 9% higher than those for the BC, respectively. This is attributed to the following rationale: the GN-reinforced gradient interphase probably provides an effective shield against interface oxidation, aids in the efficient transfer of interfacial thermal stress, and restricts the movement of the different phases of the materials at the composite interface. The study illustrates that the GN-reinforced gradient interface can efficiently improve the TOS of the 3D-4Dir braided carbon fiber/epoxy composites.

#### Acknowledgement

The authors wish to acknowledge the sponsorship of Tianjin Municipal Science and Technology Commission, China (Nos.10SYSYJC27800, 11ZCKFSF00500, and 13TXSYJC40500).

#### References

- [1] D.Q. Vu, M. Gigliotti, M.C. Lafarie-Frenot, Experimental characterization of thermo-oxidation-induced shrinkage and damage in polymer-matrix composites, *Compos. Part A* 43 (2012) 577–586.
- [2] A. Skontorp, Isothermal High-temperature Oxidation, Aging and Creep of Carbon-fiber/polyimide Composites, Ph.D. thesis, University of Houston, 1995.
- [3] M.S. Madhukar, K.J. Bowles, D.S. Papadopoulos, Thermo-oxidative stability and fiber surface modification effects on the inplane shear

- properties of graphite/PMR-15 composites, *J. Compos. Mater.* 31 (1997) 596–618.
- [4] J. Liu, X. Zhu, Z. Zhou, L. Wu, L. Ma, Effects of thermal exposure on mechanical behavior of carbon fiber composite pyramidal truss core sandwich panel, *Compos. Part B* 60 (2014) 82–90.
- [5] L.L. Song, J.L. Li, Effects of heat accelerated aging on tensile strength of three dimensional braided/epoxy resin composites, *Polym. Compos.* 33 (2012) 1635–1643.
- [6] W. Fan, J.L. Li, D.D. Guo, Effect of thermo-oxidative aging on three-dimensional and four-directional braided carbon fiber/epoxy composite, *J. Compos. Mater.* (2014), <http://dx.doi.org/10.1177/0021998314561067>.
- [7] K.J. Bowles, M. Madhukar, D.S. Papadopoulos, L. Inghram, L. McCorkle, The effects of fiber surface modification and thermal aging on composite toughness and its measurement, *J. Compos. Mater.* 31 (1997) 552–579.
- [8] X.L. Yang, Z.C. Wang, M.Z. Xu, R. Zhao, X.B. Liu, Dramatic mechanical and thermal increments of thermoplastic composites by multi-scale synergetic reinforcement: carbon fiber and graphene nanoplatelet, *Mater. Des.* 44 (2013) 74–80.
- [9] F. Yavari, M.A. Rafiee, J. Rafiee, Z.Z. Yu, N. Koratkar, Dramatic increase in fatigue life in hierarchical graphene composites, *ACS Appl. Mater. Interfaces* 2 (2010) 2738–2743.
- [10] X. Zhang, X. Fan, C. Yan, H. Li, Y. Zhu, X. Li, L. Yu, Interfacial micro-structure and properties of carbon fiber composites modified with graphene oxide, *ACS Appl. Mater. Interfaces* 4 (2012) 1543–1552.
- [11] L. Chen, H. Jin, Z.W. Xu, J.L. Li, Q.W. Guo, M.J. Shan, C.Y. Yang, Z. Wang, W. Mai, B.W. Cheng, Role of a gradient interface layer in interfacial enhancement of carbon fiber/epoxy hierarchical composites, *J. Mater. Sci.* 50 (2015) 112–121.
- [12] X. Sun, C.J. Sun, Mechanical properties of three-dimensional braided composites, *Compos. Struct.* 65 (2004) 485–492.
- [13] W. Fan, J.L. Li, Rapid evaluation of thermal aging of a carbon fiber laminated epoxy composite, *Polym. Composite.* 35 (2014) 975–984.
- [14] O. Akhavan, E. Ghaderi, R. Rahighi, Toward single-DNA electrochemical biosensing by graphene nanowalls, *ACS Nano.* 6 (2012) 2904–2916.
- [15] F. Zhao, Y.D. Huang, L. Liu, Y.P. Bai, L.W. Xu, Formation of a carbon fiber/polyhedral oligomeric silsesquioxane/carbon nanotube hybrid reinforcement and its effect on the interfacial properties of carbon fiber/epoxy composites, *Carbon* 49 (2011) 2624–2632.
- [16] M. Munz, H. Sturm, E. Schulz, G. Hinrichsen, The scanning force microscope as a tool for the detection of local mechanical properties within the interphase of fibre reinforced polymers, *Compos. Part A* 29 (1998) 1251–1259.
- [17] H. Wu, L.T. Drzal, Graphene nanoplatelet paper as a light-weight composite with excellent electrical and thermal conductivity and good gas barrier properties, *Carbon* 50 (2012) 1135–1145.
- [18] G. Schoeppner, G. Tandon, E. Ripberger, Anisotropic oxidation and weight loss in PMR-15 composites, *Compos. Part A* 38 (2007) 890–904.
- [19] D.A. Dikin, S. Stankovich, E.J. Zimney, R.D. Piner, G.H.B. Dommett, G. Evmenenko, S.T. Nguyen, R.S. Ruoff, Preparation and characterization of graphene oxide paper, *Nature* 448 (2007) 457–460.
- [20] J. Schuster, D. Heider, K. Sharp, M. Glowania, Thermal conductivities of three-dimensionally woven fabric composites, *Compos. Sci. Technol.* 68 (2008) 2085–2091.
- [21] R. Polansky, V. Mentlik, P. Prosr, J. Susir, Influence of thermal treatment on the glass transition temperature of thermosetting epoxy laminate, *Polym. Test.* 28 (2009) 428–436.
- [22] Y.M. Pei, K. Wang, M.S. Zhan, W. Xu, X.J. Ding, Thermal-oxidative aging of DGEBA/EPN/LMPA epoxy system: chemical structure and thermal–mechanical properties, *Polym. Degrad. Stabil.* 96 (2011) 1179–1186.
- [23] G. Tandon, K. Pochiraju, G. Schoeppner, Thermo-oxidative behavior of high-temperature PMR-15 resin and composites, *Mat. Sci. Eng. A* 498 (2008) 150–161.
- [24] X. Colin, A. Mavel, C. Marais, J. Verdu, Interaction between cracking and oxidation in organic matrix composites, *J. Compos. Mater.* 39 (2005) 1371–1389.
- [25] S. Marouani, L. Curtil, P. Hamelin, Ageing of carbon/epoxy and carbon/vinylester composites used in the reinforcement and/or the repair of civil engineering structures, *Compos. Part B* 43 (2012) 2020–2030.
- [26] J. Wolfrum, S. Eibl, L. Lietch, Rapid evaluation of long-term thermal degradation of carbon fibre epoxy composites, *Compos. Sci. Technol.* 69 (2009) 523–530.
- [27] T.A. Bullions, J.E. McGrath, A.C. Loos, Thermal-oxidative aging effects on the properties of a carbon fiber-reinforced phenylethynyl-terminated poly(etherimide), *Compos. Sci. Technol.* 63 (2003) 1737–1748.